ELSEVIER

Journal of Marine Systems 6 (1995) 301-312

JOURNAL OF MARINE SYSTEMS

Near-inertial motions in the coastal ocean

J. Tintoré [a,*], D.-P. Wang [b], E. García [c], A. Viúdez [a]

[a] *Dep. de Física, Universitat de les Illes Balears, E-07071 Palma, Spain*
[b] *Marine Sciences Research Center, SUNY at Stony Brook, NY 11794, USA*
[c] *Dep. de Física, Universidad Autónoma de Barcelona, E-08193 Bellaterra, Spain*

Received 22 March 1993; accepted 9 November 1994

Abstract

Internal-inertial waves are frequently observed in the upper ocean and below the thermocline. A three-dimensional general circulation model with turbulence-closure mixed layer is used to study the generation and propagation of near-inertial motion below the mixed layer. In particular, the problem of effect of a coastal wall on the wind induced inertial-internal wave field is re-examined using a fully nonlinear model. Responding to a wind pulse, a sharp wavefront propagates offshore. After the wavefront passage, strong near-inertial internal waves, marked by the tilting velocity isolines and the interface oscillations, are generated. The predicted near-inertial motion is consistent with the wave dispersion relation. Downward energy propagation occurs after the wavefront passage, and both kinetic and potential energy are strongly modified. After several inertial periods, the kinetic energy in the upper layer can be completely removed. The theoretical results, which are supported by observations, indicate that internal-inertial wave are important for mixing in the upper coastal ocean.

1. Introduction

Near inertial motions are frequently observed in the upper ocean. They are generated primarily by the local wind forcing, and their strong vertical shears are a major energy source available for vertical mixing (Pollard, 1980; Kunze and Sanford, 1984). According to the basic internal-inertial wave theory, the inertial motions most likely will be confined to the mixed layer. However, presence of inertial waves below the mixed layer has been clearly documented (Leaman, 1976; Price, 1983). The deep inertial motion is highly intermittent, and is usually characterized by upward phase propagation (or downward energy propagation); the energy source, however, is difficult to identify.

Strong inertial oscillations also have been observed near the coast. Millot and Crepon (1981) observed inertial oscillations in the Gulf of Lions (northwestern Mediterranean). Anderson et al. (1983) observed substantial inertial oscillations of 20 cm/s amplitudes off the Oregon coast. Schahinger (1988) found inertial motions at offshore site, but little oscillations at a nearshore site off Australia. Salat et al. (1992) also found strong inertial oscillations in the upper layer and below the thermocline, off the northeast Spanish coast. Furthermore, Millot and Crepon (1981) found that inertial currents were 180° out of phase between the upper and the lower layers. In

* Corresponding author.

SSDI 0924-7963(94)00030-1

the upper layer, the current oscillations had frequencies close to f, while in the lower layer the currents showed a broad peak with frequencies higher than f.

The effect of coastline on inertial motions was theoretically studied by Klinck et al. (1981), Millot and Crepon (1981), Kundu et al. (1983) and Kundu (1986). Millot and Crepon (1981), using a two layer model of an inviscid ocean, obtained analytical solution for the evolution of surface and interface elevations generated by a uniform, impulsely started cross-shore wind. They showed that the coastally generated interface oscillations have frequencies higher than f and propagate offshore at a speed close to the speed of long baroclinic wave, $C_i = [g(\rho_2 - \rho_1)h_1 h_2/\rho_2 H]^{1/2}$. They also found that, in the limit of $ft \to \infty$, the horizontal velocities are 180° out of phase between upper and lower layers. In other words, their study showed that near-inertial baroclinic motions are excited by a wave front propagating offshore and generated as a result of the flow adjustment at the coast.

Klinck et al. (1981) studied a general case of oceanic response to a moving storm. They showed that the oceanic response to a moving atmospheric front is wavelike if the speed of the atmospheric forcing U is higher than the internal wave speed C_i. Typically, this condition is always met, and two sets of internal-inertial waves are produced. One set of waves is directly forced by the horizontal variation of the Ekman suction (due to the curl of wind stress) and travels with the storm. The other set of waves arises from the reflection at the coastal wall of the directly forced waves. The coastally excited internal waves radiate away with slowly decreasing amplitude and with frequencies tending towards the inertial frequency. Gill (1984) used a similar idea to explain the generation of deep inertial waves in the open ocean. He suggested that in the wake of a storm, a divergent mixed layer will induce vertical motion at the base of the mixed layer (inertial pumping). In that case, the forcing is local, and the horizontal scale is determined by the dimension of the storm.

Millot and Crepon (1981) did not consider the transient phase of the adjustment process. This aspect was examined in Kundu et al. (1983) for a continuously stratified ocean using the normal mode approach. Similar to Millot and Crepon (1981), their results showed that the internal-inertial motions are excited by the passage of wave fronts. Furthermore, they showed that in the deep interior there are small inertial motions originated from the downward propagation of near-surface inertial waves at the coast. Later, using a two dimensional numerical model with a turbulence closure, Kundu (1984) obtained essentially the same results as in the analytical model. While Kundu et al. (1983) obtained the solution for the entire adjustment period, they did not evaluate the behavior of internal waves. More recently, Kundu (1986) used a linear two-dimensional, continuously stratified model to show that the combined effect of coastline and superposition of forcing induced much larger subsurface inertial oscillations. However, the deep inertial motion in his model was still too small to have impact on the overall energy balance.

Based on these studies, it is clear that internal waves of near-inertial frequencies can be generated by the coastal divergence or by a travelling storm. Since these waves have non-zero vertical group velocity, they will propagate away from the nearsurface. Conceivably, the internal-inertial waves will carry away a significant fraction of the surface energy, and can affect the energy exchange between the mixed layer and the interior (Gill, 1982). For example, in the classical Rossby adjustment problem, two thirds of the potential energy released is carried away with the waves. Therefore, it is important to understand the role of near-inertial motion in the flow adjustment. In this study, we re-examine the problem of generation of inertial-internal wave by the coastal divergence, with special emphasis on the transfer of energy from the mixed layer to the interior.

2. Numerical model formulation

The model used is described in Wang (1985, 1990). It is a three-dimensional, primitive-equation model with an embeded mixed layer of second-order turbulence closure. Since we are mostly interested on the offshore/vertical propagation of near-inertial energy, we simplified the physical domain by considering a vertical cross-shore section as study area. It is important to note that the model is fully non-linear and that the hydrostatic approximation is justified since the focus is given on waves with frequencies much lower than the Brunt–Vaisala frequency.

2.1. Basic equations

The governing equations are

$$\frac{\partial u}{\partial t}+u\frac{\partial u}{\partial x}+w\frac{\partial u}{\partial z}-fv = -\frac{1}{\rho}\frac{\partial p}{\partial x}+\frac{\partial}{\partial x}\left(A_h\frac{\partial u}{\partial x}\right)+\frac{\partial}{\partial z}\left(A_v\frac{\partial u}{\partial z}\right) \quad (1)$$

$$\frac{\partial v}{\partial t}+u\frac{\partial v}{\partial x}+w\frac{\partial v}{\partial z}+fu = \frac{\partial}{\partial x}\left(A_h\frac{\partial v}{\partial x}\right)+\frac{\partial}{\partial z}\left(A_v\frac{\partial v}{\partial z}\right) \quad (2)$$

$$\frac{\partial p}{\partial z}+\rho g=0 \quad (3)$$

$$\frac{\partial u}{\partial x}+\frac{\partial w}{\partial z}=0 \quad (4)$$

$$\frac{\partial \rho}{\partial t}+u\frac{\partial \rho}{\partial x}+w\frac{\partial \rho}{\partial z}=\frac{\partial}{\partial x}\left(K_h\frac{\partial \rho}{\partial x}\right)+\frac{\partial}{\partial z}\left(K_v\frac{\partial \rho}{\partial z}\right) \quad (5)$$

where t is time, x, y and z the space coordinates, u and v the x- and y-components of the current velocity (offshore, alongshore), ρ is density, f the Coriolis parameter.

A detailed description of the model can be found in Wang (1982). The numerical technique is standard for three-dimensional multi-level models. In essence, Eqs. (1)–(5) are written in finite-difference form in a staggered grid. The scheme is leapfrog in time, centered in space (except for the density equation where a flux corrected transport scheme is used). It uses mode-split in the vertical direction and a semi-implicit scheme in the horizontal direction to achieve computational efficiency.

Horizontal eddy coefficients A_h, K_h are constant (10^5 cm^2/s) while the vertical eddy coefficients A_v, K_v are computed from the mixed layer model of Chen and Wang (1990) as:

$$(A_v, K_v) = lq(S_M+\nu_M, S_H+\nu_H) \quad (6)$$

The terms involving ν account for the background viscosity and background diffusion. l is the mixing length, q the square root of twice the turbulence kinetic energy, and S_M and S_H are functions of the gradient Richardson number

$$Ri = \frac{\frac{g}{\rho}\frac{\partial \rho}{\partial z}}{\left(\frac{\partial u}{\partial z}\right)^2+\left(\frac{\partial v}{\partial z}\right)^2} \quad (7)$$

When Ri exceeds a critical value (0.23), $S_M = S_H = 0$, and turbulent mixing is suppressed by the density stratification. q is computed from a stationary turbulence energy equation and l following the vertical distribution of q. Details on the mixed-layer formulation can be found in Chen and Wang (1990).

The mixed layer implementation is as follows. The vertical eddy coefficients A_v, K_v are computed directly from the mixed layer model and are then fed back to the GCM. In this approach, the turbulent kinetic energy available for mixing comes only from the one-dimensional mixed layer model. To examine the inviscid limit of the initial adjustment, the background viscosity is set to a small number (0.1 cm^2/s).

2.2. Initial and boundary conditions

Model domain is a cross section from the coast to 60 km offshore (20 grid points), flat bottom and has 20 vertical layers (3 m each). The model latitude is 41° north where the local inertial frequency is $f = 9.5 \times 10^{-5}$ s^{-1} (period $T = 18.29$ h). Boundary conditions are as follows. At the sea surface $z = \xi$,

$$A_v\left(\frac{\partial u}{\partial z}, \frac{\partial v}{\partial z}\right) = (\tau_x, 0)$$

where τ_x is the cross-shore component of wind stress. At the bottom, $z = -H$,

$$A_v\left(\frac{\partial u}{\partial z}, \frac{\partial v}{\partial z}\right) = C_D(u,\nu)(u^2+\nu^2)^{1/2}$$

where the C_D, a drag coefficient is 3×10^{-3}. At the coast, $x = 0$, the normal flow and the normal fluxes of momentum and density vanish. Finally, at the open ocean, a radiation condition was used.

The initial density profile is typical of the summer condition off the northeast Spanish coast (Fig. 1). The phase speeds for the first two baroclinic modes associated with this initial density profile are 25 cm/s and 13 cm/s, obtained by solving the eigenvalue problem of the normal mode equation. The model is run with a 15 m/s offshore wind pulse from 0 to 8 h (the drag coefficient is 1.67×10^{-3}). The wind pulse also is typical of the devastating events frequently observed during the otherwise quiescent summer season off northeast Spain. This type of wind pulses is associated with the travelling atmospheric fronts characterized by speeds of about 5 m/s. Since the speed of the atmospheric forcing is higher than the speed of long baroclinic waves, a wavelike oceanic response is expected. The model results, however, do not depend on the nature of wind forcing.

3. Results

During the wind pulse, a well defined mixed layer of approximately 12 m deep rapidly develops, and a strong offshore current driven directly by the wind stress is confined to the mixed layer. Fig. 2a and b shows the cross-shore velocity at 6 km and 12 km off the coast. The response is essentially uniform in the cross-shore direction; in other words, the initial mixed-layer deepening is a one-dimensional (vertical) process. The only exception is near the coast (e.g. at 6 km offshore, Fig. 2a) where the velocity increase is affected by the coastal wall which inhibits normal flow. Fig. 3a and b shows the corresponding density time series at 6 km and 12 km offshore. The upwelling can be readily seen in Fig. 3a as the thermocline rises during the wind pulse. The width of the upwelling zone usually is defined by the baroclinic deformation radius (c_i/f) which is about 3 km. The model calculation shows that the upwelling influence can be felt to about 10 km offshore; the difference is a factor π usually dropped out in the scale analysis (Gill, 1982, p. 155). If the wind forcing would last longer, an upwelling front will form which can strongly interact with the mixed layer. This problem was examined by Chen and Wang (1990) for the coastal upwelling area off central California (CODE study), and will not be addressed here.

Immediately after the wind pulse, a rapid barotropic adjustment associated with the passage of the surface gravity wave, establishes a homogeneous flow in the lower layer such that the total cross-shore transport is essentially zero. This response is uniform in the cross-shore direction, and is a unique property of the coastal response. It should be noted that motion with zero-transport does not necessarily mean an internal wave. This is quite evident at the offshore (12 km) site (Fig. 3b) where the pycnocline shows no vertical movement during the first 30 h.

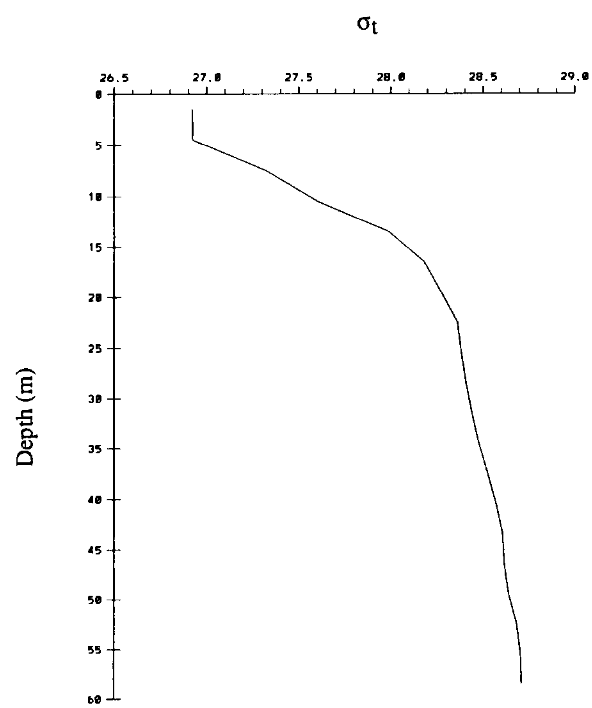

Fig. 1. Density profile used as initial condition in the numerical simulation. This profile corresponds to station 40 of the FE87 cruise (June 1987) in the shelf region off the northeast Spanish coast.

At the nearshore (6 km) site, significant isopycnal oscillations start to occur at about 20 h (Fig. 3a). The pycnocline rises by about 10–15 m during the first half inertial period, and large interface oscillations prevail through the simulation period. These large interface oscillations indicate the presence of internal waves of near-inertial period. The period of these oscillations tends to increase with time. For example, the first cycle has a rather short period of about 15 h. Based on the maximum entropy spectrum analysis of model results for the entire simulation period, the period of oscillation is 17.6 h, or about 5% higher than the local inertial frequency. Coincidental with the presence of large interface oscillations the cross-shore velocity profile also shows drastic change. At about 20 h, the phase lines start to tilt upward (Fig. 2a), and the velocity amplitude in the mixed layer starts to decrease. Indeed, the maximum amplitude has shifted downward well below the mixed layer at the end of simulation period. This is clear evidence of the downward propagation of inertial energy, characterized by the upward phase propagation of inertial-internal wave.

The situation at the 12 km site is strikingly different from that at the 6 km site. Before 35 h, while large internal waves have already appeared nearshore, the offshore site sees no internal wave motion. The pycnocline is flat and the mixed-layer velocity has a constant amplitude. However, a sharp drop of interface occurs at about 40 h, and simultaneously, the velocity phase lines start to tilt (Fig. 2b). The effect of the coastal wall is felt at even later time at the 20 km site.

For near-inertial waves, the particle trajectory is almost circular. Fig. 4 shows the phase ($\tan^{-1} u/v$) time series at the base of the mixed layer (depth = 23 m) for three different sites, 6, 12 and 18 km from the coast. Initially, motions at all

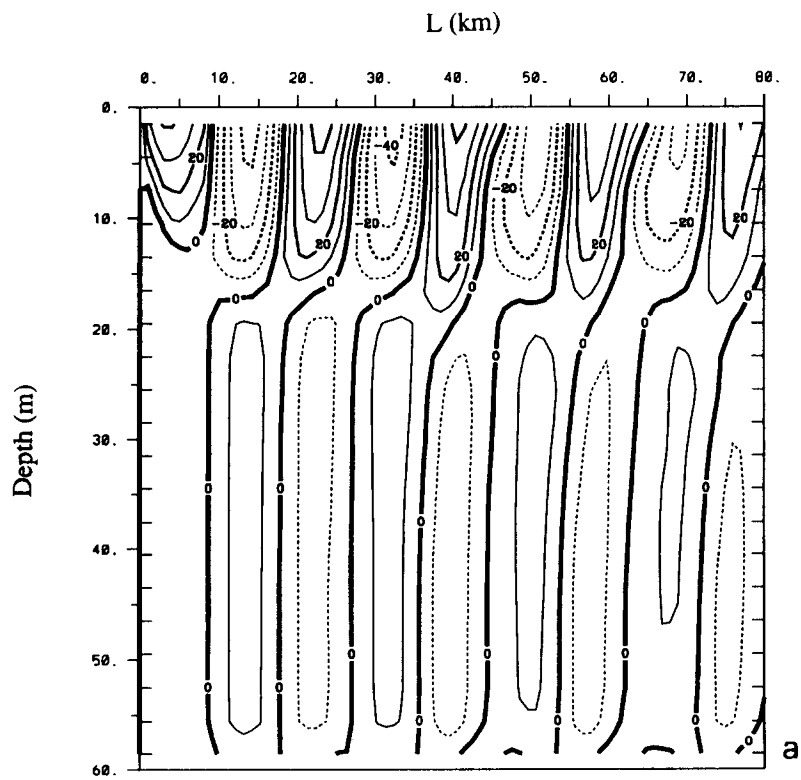

Fig. 2. (a) Time evolution of the vertical distribution of the cross-shore horizontal velocity at a coastal site located 6 km offshore. (b) Time evolution of the vertical distribution of the cross-shore horizontal velocity at 12 km offshore.

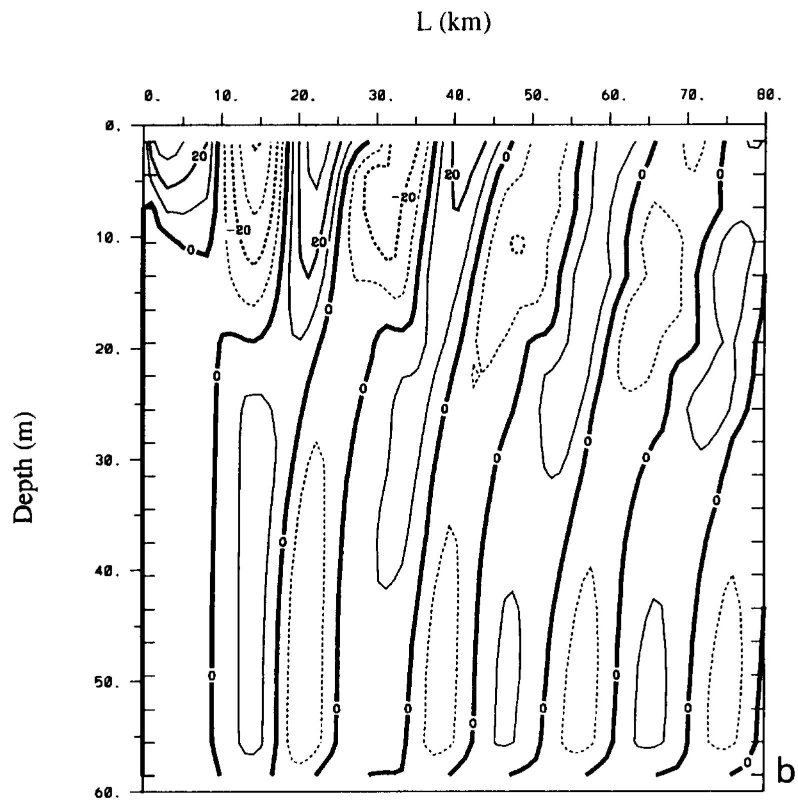

Fig. 2 (continued).

three sites are in phase with a linear phase change (constant period equal to the local inertial period). At 18 h, significant changes in phase appear nearshore, indicating the presence of internal waves. This phase modification is more clearly seen at the 12 km site where the change occurs at 38 h, coinciding with the start of the isopycnal oscillations (Fig. 3). The sudden phase change is associated with the arrival of the wavefront, and afterwards, the phase slope increases indicating that the frequencies become higher than f. After several inertial periods, the phase lines become again paralel to the local inertial period.

To establish the offshore progression of the internal waves, Fig. 5 shows the density evolution at the depth of the pycnocline (depth = 18 m). During the wind pulse, the upwelling zone is within the first 10 km. The interface oscillations appear at the coast immediately after the wind pulse, and the fluctuations gradually spread offshore. The wave front, that is, the first steep interface drop, travels at a speed of approximately 10 cm/s. Since this is the speed of propagation of the whole pattern (the group), it is by definition the group speed, C_g. The phase velocity can also be estimated from the slope of the lines of constant phase, and it is about 40 cm/s. The vertical group velocity can be estimated from the downward displacement of the velocity maxima in Fig. 2b, and we obtain $C_{gz} = 22$ m/day (or 0.025 cm/s). Also, from the tilting of velocity isolines in Fig. 2b, the vertical phase velocity is about 90 m/day, or $C_{pz} = 0.1$ cm/s.

4. Verification of dispersion relation

For vertically propagating inertial-internal waves, the dispersion relation under hydrostatic assumption is

$$\omega^2 = f^2 + N^2 \alpha^2 \tag{10}$$

where a constant N^2 is assumed, and $\alpha = k/m$, the aspect ratio. From the initial density profile, we can estimate an averaged Brunt–Vaisala frequency $N^2 = 3.5 \times 10^{-4}$ s^{-2}. Also, since the estimated horizontal and vertical phase velocities are 40 cm/s and 0.1 cm/s, we can estimate the aspect ratio $\alpha = k/m = C_{pz}/C_{px} = 0.002$. From Eq. (10) we can therefore obtain $\omega = 1.06 \times 10^{-4}$ s^{-1} (16.5 h) which implies that the internal wave frequency is 11% higher than the local, inertial period ($\omega/f = 1.11$). The horizontal wavenumber $K = \omega/C_{px} = 2.65 \times 10^{-6}$ cm^{-1} and the associated wavelength $\lambda_x = 24$ km. Similarly, the vertical wavenumber $m = \omega/C_{pz} = 1.06 \times 10^{-3}$ cm^{-1}, corresponding to a vertical wavelength $\lambda_z = 59$ m.

For vertically propagating waves, the dispersion relation implies that (Gill, 1982, pp. 260–262):

$$C_{gz} = \frac{N^2\alpha^3}{k(f^2 + N^2\alpha^2)^{1/2}} \tag{11}$$

$$C_{gx} = \frac{N^2\alpha}{m(f^2 + N^2\alpha^2)^{1/2}} \tag{12}$$

Our estimated horizontal and vertical group velocities are fully consistent with Eqs. (11), (12), if N^2 is chosen equal to 3.5×10^{-4} s^{-2} which is a reasonable value since it is actually the mean value corresponding to the observed density profile used as initial condition.

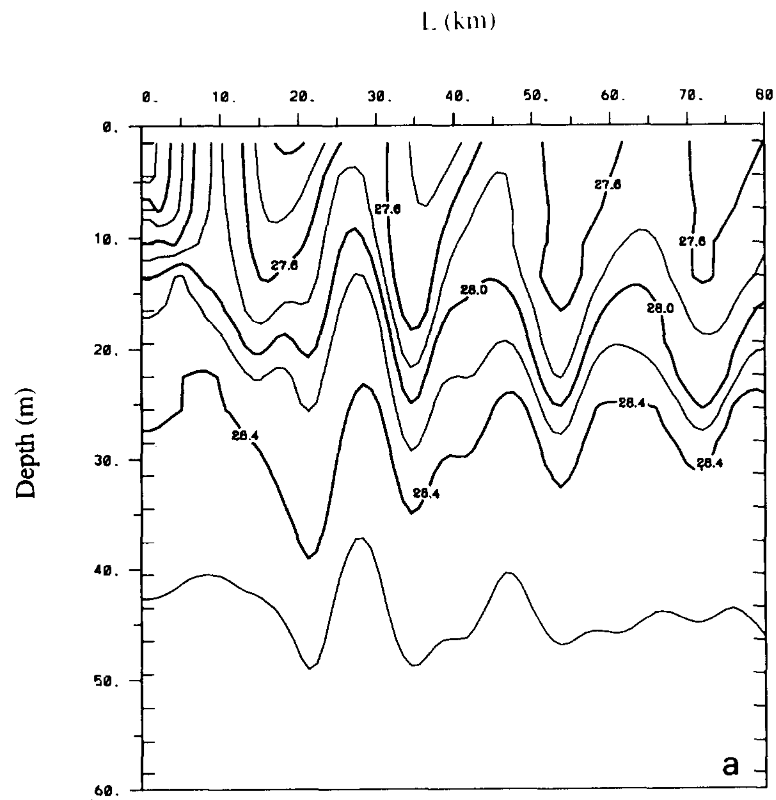

Fig. 3. (a) Time evolution of the vertical distribution of density near the coast, 6 km offshore. (b) Time evolution of the vertical distribution of density 12 km offshore.

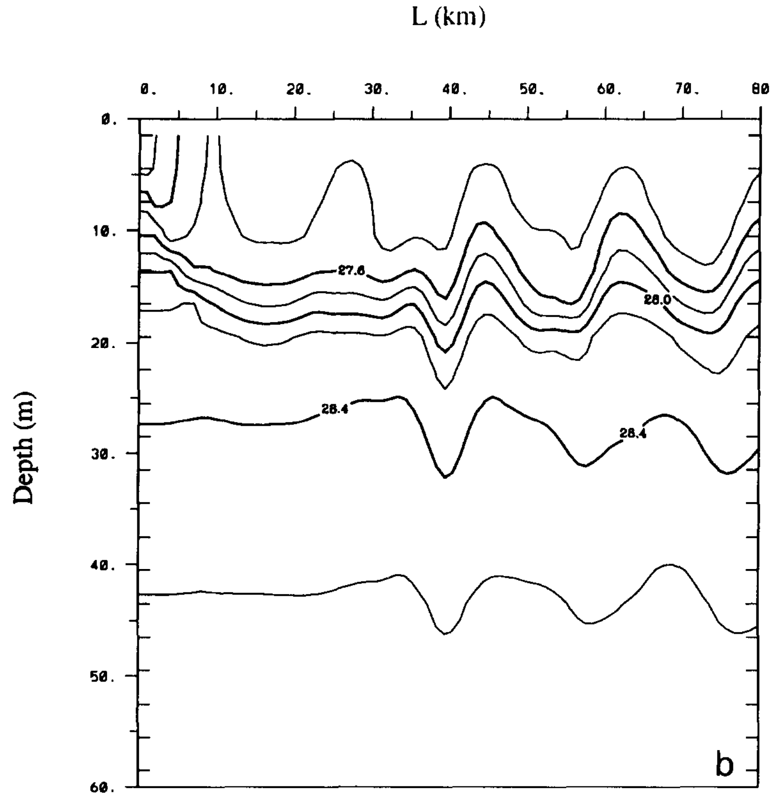

Fig. 3 (continued).

5. Energy propagation

We have shown that a transient wind forcing in the presence of a coastal boundary induces the offshore propagation of a wave front. Once the wave front has passed, near-inertial motion appears in the lower layer as a result of the downward propagation of internal-near inertial wave energy. We have also shown that the calculated internal waves agree well with the elementary wave dispersion relation. In this section we study in detail the energy transfer between upper and lower layer.

To confirm the relationship between wavefront passage and downward energy propagation, we computed the kinetic energy of the internal-inertial waves defined as:

$$KE = \frac{1}{2}\langle (u - \langle u \rangle)^2 + (v - \langle v \rangle)^2 \rangle \tag{13}$$

where the brackets mean average over one inertial period. Fig. 6 shows the kinetic energy (KE) at the 12 km site both at the surface and in the lower layer (20 m). During the first inertial period, the kinetic energy in the upper layer is considerably higher than below with values in the range of 700 and 25 erg, respectively. After the second inertial period, there is a rapid depletion of KE at the surface that coincides with a significant increase of KE below the thermocline. This suggests the kinetic energy associated with the wavefront is at least partially radiated downward from the surface to deeper layers. Also note that since the wavefront passage induce significant oscillations of the density field, the potential energy field is affected.

According to the linear theory, the PE is much smaller than the KE for the near-inertial motion. On the other hand, associated with the wavefront passage, the computed ratio of KE/PE is approximately equal to 10, suggesting therefore that non linear density-vertical velocity interactions (in the density equation) do play a significant role in the energy exchange between the upper layer and the thermocline. An important point needs to be emphasized since the main difference between our work and the linear theory lies in the fully non-linear density equation which is used in this simulation and which allows for a non linear coupling between the density field and the vertical velocity. In other words, for a linearised density equation, the vertical velocity is always out of phase with the density fluctuation and consequently $< w\rho >$ is always zero. This has important dynamic implications since then the kinetic energy cannot be converted into potential energy. In our model, due to nonlinear coupling, $< w\rho >$ does not vanish, which therefore might result in an increase of potential energy.

Summarizing, Fig. 6 essentially implies that upper-layer kinetic energy moves donward. However, it is important to analyze if this is a local process, or if after sometime, the lower layer (in all the domain) is affected. In consequence, we study the time evolution of *KE*. Fig. 7a (note logarithmic scale) shows that during the first inertial cycle, the kinetic energy is mostly reduced to the upper layer. During the second inertial period, (7b), a significant energy maxima appears below the mixed layer at approximately 10 km offshore. Five inertial cycles later, a significant increase in lower layer energy has taken place in almost all the domain (Fig. 7c and d)

6. Discussion

Comparison with previous studies indicate that the rate of energy transfer between the upper and lower layer (as measured by C_{gz}) is in the range of values described by Brooks (1983) who obtained $C_{gz} = 60$ m/day or by Kundu et al.

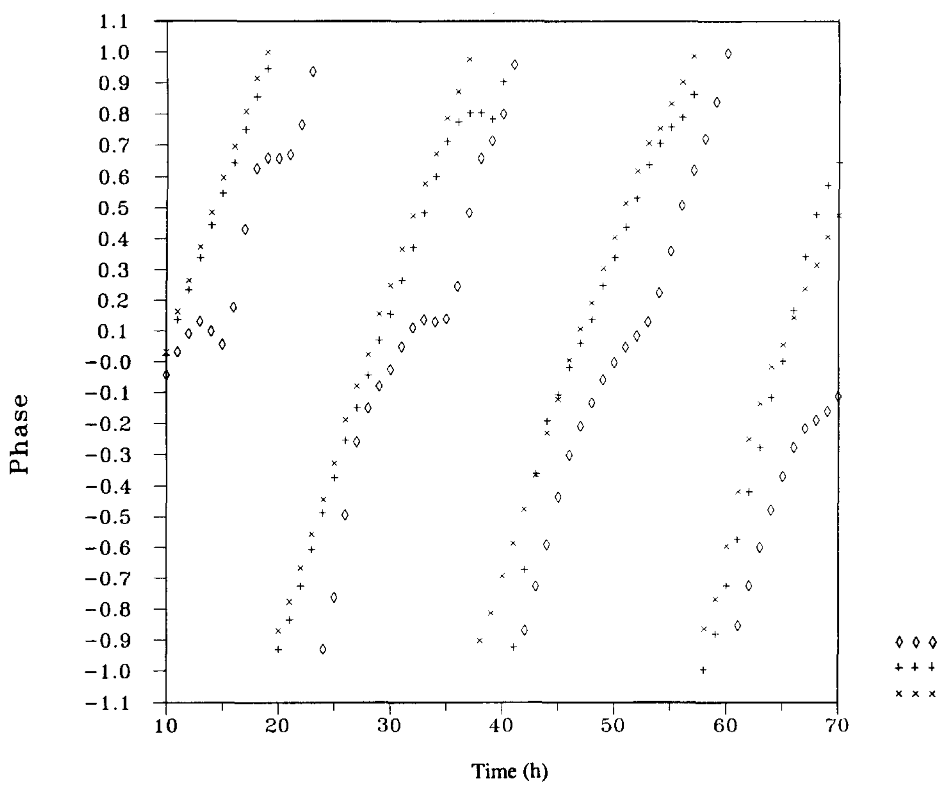

Fig. 4. Time serie of the phase below the mixed layer (18 m) and at 6 (◇), 12 (+) and 18 (×) km offshore.

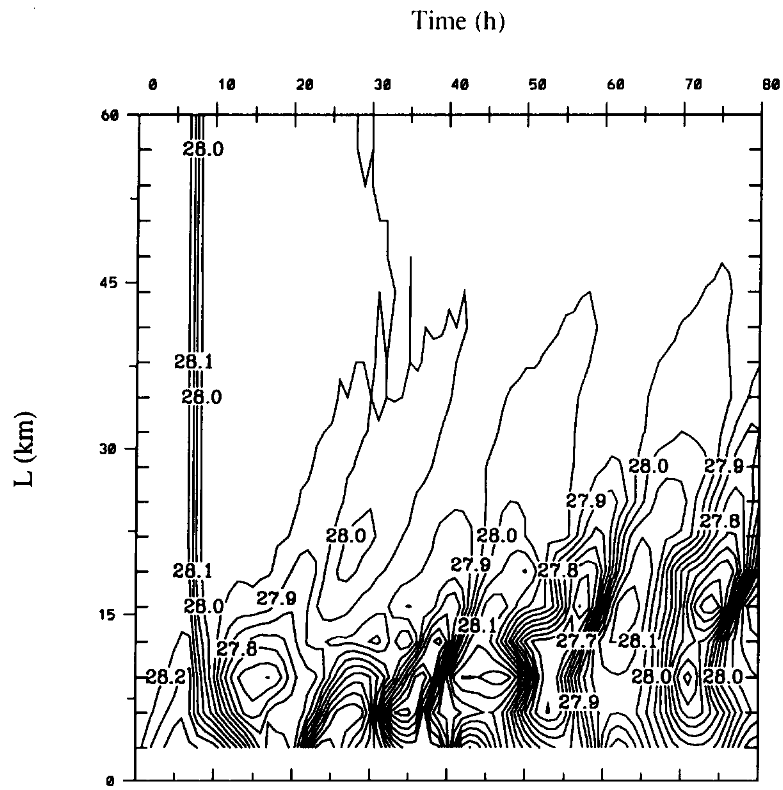

Fig. 5. Time evolution of the cross-shore horizontal density distribution at a depth of 18 m (layer 6, pycnocline).

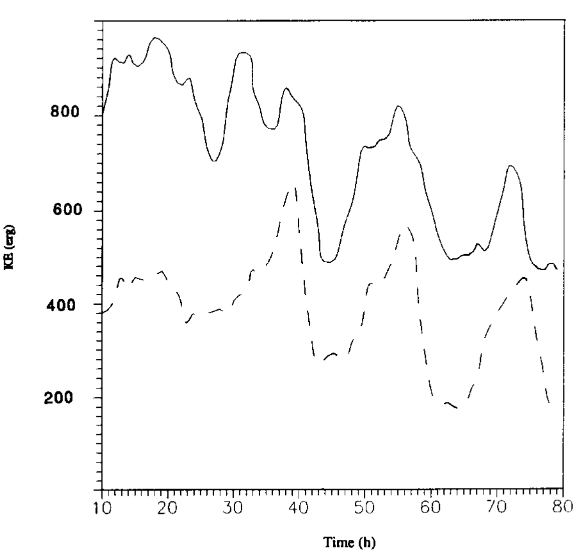

Fig. 6. Time serie of the kinetic energy averaged in every inertial period at the surface (plain) and at 20 M (dashed) at 12 km offshore.

(1983) found $C_{gz} = 45$ m/day. It is important to note that the velocity values we obtained below the mixed layer, after the wind pulse agree quite well with currentmeter observations off the northeast Spanish coast in June 1987 (Salat et al., 1992) which suggests that we have correctly simulated the energy exchange between the upper layer and the thermocline in the coastal ocean.

Most previous observations suggested that the near-inertial motion on the shelf is a standing baroclinic wave. However, Wang and Mooers (1977), based on observations from a coastal upwelling study off Orgeon found a strong inertial beam in the subsurface after a wind event. They suggested that the subsurface inertial energy was generated earlier in the nearsurface. They estimated that the horizontal and vertical wavelengths are 15 km and 60 m, and the vertical group velocity is 17 m/day. These values compare well with our theory, supporting the notion that radiation of inertial-internal waves is effective in removing the surface inertial energy. It is also important to note that the near-inertial oscillations described in our study have significant effects on the vertical excursion of particles and as a result, might also modify the depth distribution of primary production (Holloway, 1984; Holloway and Denman, 1989).

In summary, our numerical study in the coastal ocean shows that responding to a wind pulse, a sharp wavefront propagates offshore and strong near-inertial waves are generated. The wavefront passage induces modification of kinetic and potential energy therefore modifying the vertical distribution of biogeochemical variables. Results also indicated much more rapid depletion of the mixed-layer inertial energy near the coast. For example, at 6 km offshore, the energy decreased

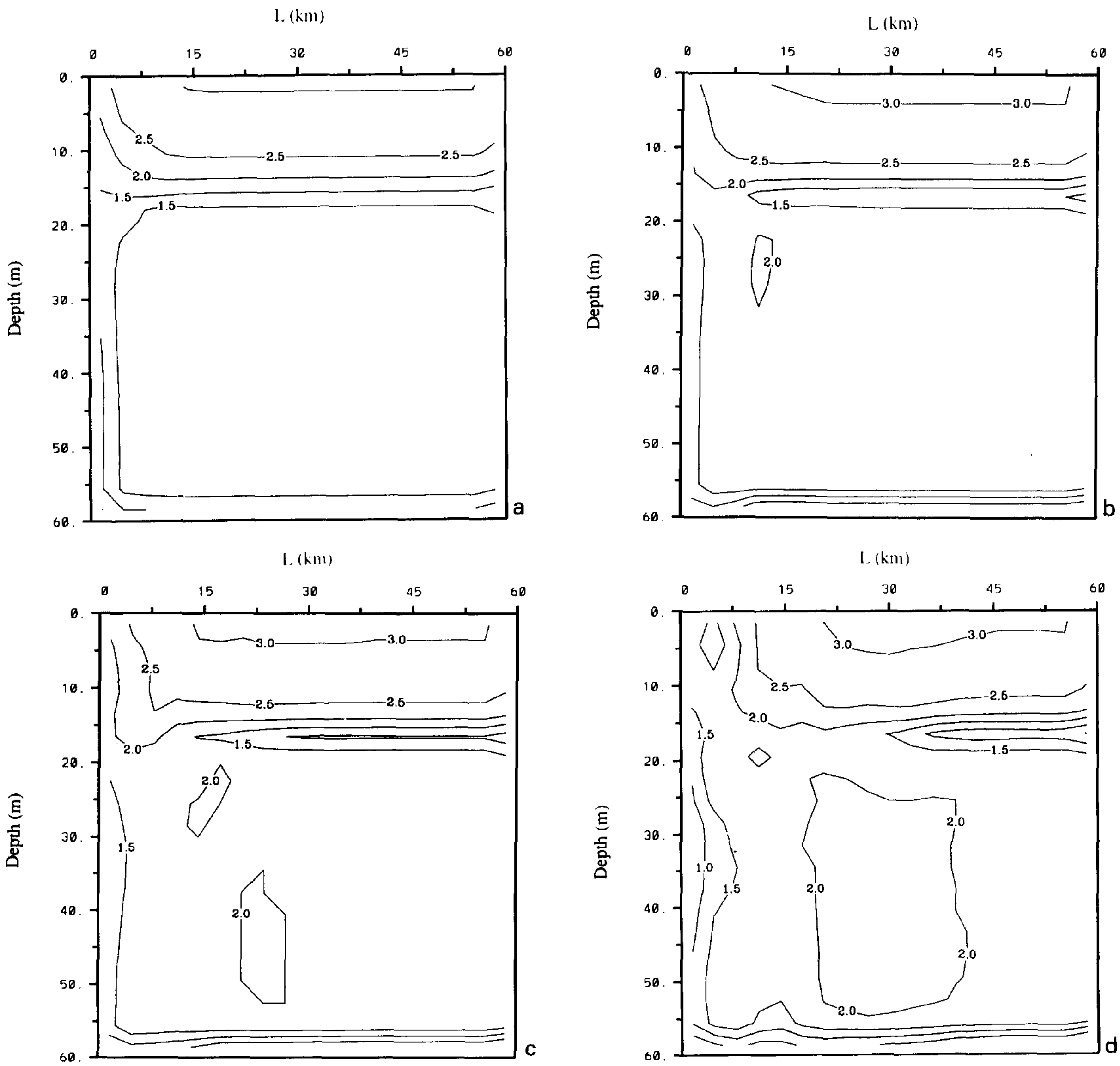

Fig. 7. Kinetic energy (natural log units) averaged every 18 h (one inertial period) for the first inertial cycle (a), for the second inertial cycle (b), for the third (c) and fifth (d).

by a factor of 7 in 2 inertial periods. As a result radiation of inertial-internal waves are effective in removing the surface inertial energy. Also important is that because of the presence of internal-inertial waves, mixing in the coastal ocean cannot be treated as a one dimensional problem.

Acknowledgements

This work has been partially funded by the European Community under program MAST (Marine Applied Sciences and Technology), project EUROMODEL (MAS2-CT93-0066), the CICYT (MAR89-0550, MAR91-1492-CE, AMB93-1046-CE) and the DGICYT (PB89-0428). Part of this work was carried out while one of the authors (D.-P. W) was a visiting professor at the University of the Balearic Islands whose support is also acknowledged. Useful comments from anonymous referees are gratefully acknowledged.

References

Anderson, I., Huyer, A. and Smith, R.L., 1983. Near-inertial motions off the Oregon coast. J. Geophys. Res., 88: 5960–5972.

Brooks, D.A., 1983. The wake of hurricane Allen in the Western Gulf of Mexico. J. Phys. Oceanogr., 13: 117–129.

Chen, D. and Wang, D.-P., 1990. Simulating the time-variable coastal upwelling during CODE 2. J. Mar. Res., 48: 335–358.

Gill, A.E., 1982. Atmosphere Ocean Dynamics. Academic Press, New York, 662 pp.

Gill, A.E., 1984. On the behaviour of internal waves in the wakes of storms. J. Phys. Oceanogr., 14: 1129–1151.

Holloway, G., 1984. Effects of velocity fluctuations on vertical distributions of phytoplancton. J. Mar. Res., 42: 559–571.

Holloway, G. and Denman, K., 1989. Influence of internal waves on primary production. J. Plankton Res., 11: 409–413.

Kundu, P.K., Chao, S.Y. and McCreary, J.P., 1983. Transient coastal currents and inertio-gravity waves. Deep-Sea Res., 30(10A): 1059–1082.

Kundu, P.K., 1984. Numerical calculations of coastal flow with turbulent dynamics. Deep-Sea Res., 31(1): 39–60

Kundu, P.K., 1986. A two dimensional model of inertial oscillations generated by a propagating wind field. J. Phys. Oceanogr., 16: 1399–1411.

Kunze, E. and Sanford, T., 1984. Observations of near-inertial waves in a front. J. Phys. Oceanogr., 14: 566–581.

Klinck, J.M., Pietrafesa, L.J. and Janowitz, G.S., 1981. Continental shelf circulation induced by a moving, localized wind stress. J. Phys. Oceanogr., 11: 836–848.

Leaman, K.D., 1976. Observations of vertical polarization and energy flux of near-inertial waves. J. Phys. Oceanogr., 6: 894–908.

Millot, C. and Crepon, M., 1981. Inertial oscillations on the continental shelf of the Gulf of Lions—Observations and theory. J. Phys. Oceanogr., 11(5): 639–657.

Pollard, R.T., 1980. Properties of near surface inertial oscillations. J. Phys. Oceanogr., 10: 387–398.

Price, J.F., 1983. Internal wave wake of a moving storm. Part 1: scales, energy budget and observations. J. Phys. Oceanogr., 13: 949–965.

Salat, J., Tintoré, J., Font, J., Wang, D.-P. and Vieira, M., 1992. Inertial motion on shelf/slope front off northeast Spanish coast. J. Geophys. Res., 97(5): 7277–7281.

Schahinger, R.B., 1988. Near inertial motion on the south Australian shelf. J. Phys. Oceanogr., 18(3): 492–504.

Wang, D.P. and Mooers, C.N.K., 1977. Evidence for interior dissipation and mixing during a coastal upwelling event off Oregon. J. Mar. Res., 35(4): 700–713.

Wang, D.P., 1982. Development of a three-dimensional limited-area (island) shelf circulation model. J, Phys. Oceanogr., 12: 605–617.

Wang, D.P., 1985. Numerical study of gravity currents in a channel. J. Phys. Oceanogr., 15: 299–305.

Wang, D.P., 1990. Model of mean and tidal flows in the Strait of Gibraltar. Deep-Sea Res., 36: 1535–1548.